

Examining Electron Properties

Robert J. Pierrard

Advanced Lab PHYS 4321, Professor de Heer
Georgia Institute of Technology

October 2021

Abstract

We complete two experiments in this lab. First, we calculate the charge to mass ratio of the electron using a Helmholtz coil apparatus. Then, firing an electron gun at gold foil, we relate the produced diffraction rings to the properties of the electron. We find that $\frac{e}{m} = -2.12 \cdot 10^{11} \frac{[C]}{[kg]}$, 20% greater than the actual value of $\frac{e}{m} = -1.6 \cdot 10^{11} \frac{[C]}{[kg]}$. For the diffraction experiment, we qualitatively predict the behavior of the diffraction pattern but have very large errors when relating our theoretical calculation to experiment. Despite this, through the diffraction experiment we demonstrate that an electron can behave as a wave. As such we confirm the wave-particle duality of the electron through our experiments.

1 Introduction

The history of the electron is full of discovery. From the discovery of the existence of electric charge, to precise measurements of its characteristics, and to its behavior in electrical and chemical systems, the electron is one of the most well studied particles in physics.

Going back to the 19th century, humanity's understanding of the world around us was vastly different. Simple concepts which we have been taught from a young age, such as electrons conducting electricity (better yet the existence of electrons), were unknown to the most esteemed scientists.

In the mid 1800s, science lectures would travel from town to town to demonstrate the fluorescent glow of a cathode ray tube. They would put a high voltage across glass tubes and pump out most of the air - then people would stare in amazement. In 1859, a German physicist used an improved pump to create a better vacuum in within the glass tube. With this improved device, he could conclude that some sort of ray was being emitted by the cathode and travelling to the anode, lighting up the glass in the process. The mystery of what these rays were made of still remained [5].

A series of experiments with cathode ray tubes soon followed. When a magnet is placed near the glass of a cathode ray tube, it deflects the rays, yet Heinrich Hertz showed that when the rays pass through an electric field, they do not deflect in the normal way of an electrically charged particle. Further, the rays seemed to pass straight through thin metal foils. Concurrently, theories regarding the propagation of light were also circulating. It was known that light could behave as a wave, yet it could pass through empty space. Some concluded that light passed through a mystery medium known as the ether. It was also thought that cathode rays may pass through the same or a similar medium - perhaps they were waves [5].

Continuing with further experimentation, Jean Perrin discovered that the cathode rays are negatively charged. In 1897 Emil Wiechert measured the the charge to mass ratio of the rays was over 1000 times smaller than the ratio for the smallest charged atom [5].

Building upon his predecessors work, JJ Thomson conducted a series of experiments on cathode rays starting in 1895. He determined that the electric charge which a cathode ray carries could not be separated away from it, that cathode rays do indeed respond to electric fields if proper experimental measures are taken, and confirmed Perrin's results of the great size of the cathode rays charge to mass ratio. With these experiments, and subsequent confirmatory ones conducted by other scientists, Thomson stated the bold hypothesis that "we have in the cathode rays matter in a new state, a state which the subdivision of matter is carried very much further than in the ordinary gaseous state: a state in which all matter... is of one and the same kind; this matter being the substance from which all the chemical elements are built up." With this claim, we now credit JJ Thomson with the discovery of the electron [5].

At the time most people thought that atoms were indivisible pieces of matter. The electron was therefore the first discovered subatomic particle. Our understanding of matter was fundamentally changed [4].

In the early 1900's the properties of the electron continued to be measured in more detail and with more precision. In 1924, theoretician Louis de Broglie made a bold proposition that particles should also behave as waves. His predictions were confirmed a mere three years later in two independent experiments. One of which was conducted at Bell Labs by Clinton Davisson and Lester Germer. The so-called Davisson-Germer experiment consisted of scattering a beam of electrons by shooting them at the surface of a crystal of nickel metal. Behaving as waves, the electrons then interfere with each other and display diffraction patterns when observed [6].

In this lab we will calculate the charge-to-mass ratio of the electron by measuring the deflection of an electron beam passing through a magnetic field. Additionally, we will recreate a similar experiment to that performed at Bell Labs by firing an electron beam at a polycrystalline gold foil and observing the diffraction patterns. Along the way, we will make comments on additional properties of the electron.

Each section of this lab will be divided into two parts, one for calculating the charge-to-mass ratio and the other for characterizing the diffraction patterns.

2 Theoretical Considerations

2.1 Charge-to-mass Ratio Considerations

This subsection greatly references [1].

For calculating the charge-to-mass ratio of the electron we are firing an electron beam through a magnetic field. The magnetic force acting on a charged particle moving in a magnetic field is given by the equation

$$F_B = qv \times B \quad (1)$$

where q is the charge of the particle, v is the velocity, and B is the magnetic field. Given that this formula is a cross product, the physical geometry of the magnetic field and the trajectory of the particle influence the direction of the magnetic force.

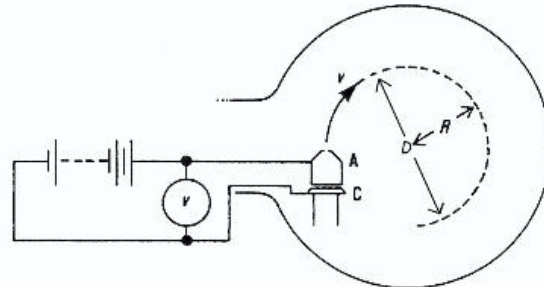


Figure 1: Schematic depicting the trajectory of an electron field passing through a uniform magnetic field directed into the page. The electron is accelerated across a potential difference from C to A and thus has an initial velocity solely in the upwards direction. Due to the Lorentz force, the electron move sin a circular pattern.

For simplicity, it is ideal if we produce a uniform magnetic field perpendicular to the velocity vector of our electron. In such a configuration, our electron will move in a circular pattern with our magnetic force being the only centripetal force.

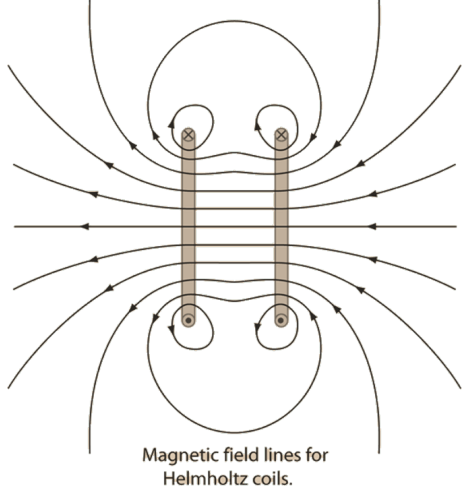


Figure 2: Magnetic field geometry between two Helmholtz coils. Note the uniformity and direction of the magnetic field in the central region. This configuration is used to generate a roughly constant magnetic field in the plane between our two coils.

With this configuration, we can write our formula for the magnetic force in its scalar form.

$$F_B = qvB \quad (2)$$

As stated, the magnetic force is the only centripetal force.

$$F_c = \frac{mv^2}{r} = F_B \quad (3)$$

$$\therefore \frac{q}{m} = \frac{v}{Br} \quad (4)$$

The simplicity of these equations raise the question of how we produce such a magnetic field geometry, there is a simple solution. There exists a roughly uniform magnetic field in the plane equidistant between two Helmholtz coils. The magnetic field is directed between the two coils (Figure 2). By firing an electron in this plane, perpendicular to the direction of the magnetic field lines, our electron beam will move in a circular arc.

In addition to requiring a uniform magnetic field, we see that our ratio in equation ?? is dependent on knowing the magnitude of our magnetic field and the velocity of our electrons.

Given our experimental apparatus, we can not directly measure the magnitude of our magnetic field at the center of our two coils. However, we know the current being supplied to the coils, as well as the physical parameters of our Helmholtz coils. Another benefit of the geometry of Helmholtz coils is that we can analytically calculate the magnetic field around the coils. The magnetic field produced near the central axis of a pair of Helmholtz coils is given by the following calculation.

Starting with the Biot-Savart Law, which relates magnetic fields to the currents which are their sources.

$$d\vec{B} = \frac{\mu_0}{4\pi} \frac{Id\vec{l} \times \hat{r}}{r^2} \quad (5)$$

If we know make our current path a closed loop and restrict ourselves to evaluating the magnetic field along the axis passing through the center of the loop, which we will denote as

the z axis, we get the following equation for the z component of the magnetic field.

$$dB_Z = \frac{\mu_0 IdL}{4\pi} \cdot \frac{R}{(z^2 + R^2)^{3/2}} \quad (6)$$

Where R is the radius or our current loop and z is the position along our z axis such that z=0 is in the plane or our current loop. We have converted from a vector equation to a scalar equation. The other components of the magnetic field cancel due to the cylindrical symmetry of our system.

All terms are constant and so the integral over dL is simply the circumference of a circle.

$$B_z = \frac{\mu_0}{4\pi} \cdot \frac{2\pi R^2}{(z^2 + R^2)^{3/2}} \quad (7)$$

$$B_z = \frac{\mu_0 IR^2}{2(z^2 + R^2)^{3/2}} \quad (8)$$

Finally, if instead we have two identical coils with currents flowing in the same direction, positioned a distance R away from each other along their z axis, we can calculate the magnetic field at the midpoint between these coils. Since the coils are identical, their magnetic field contributions will be identical at their midpoint and so we can simply scale our calculation for one coil by two.

$$B_{midpoint} = \frac{2\mu_0 IR^2}{2((\frac{R}{2})^2 + R^2)^{3/2}} \quad (9)$$

$$\therefore B_{midpoint} = \left(\frac{4}{5}\right)^{3/2} \frac{\mu_0 n I}{R} \quad (10)$$

Lastly, we have included a term n which represents the number of loops per coil. The fields of each loop superimpose and so we can simply multiply our result for one coil by n to extend our solution to the n coil case.

Finally, with equation 10 we can calculate our magnetic field on axis at the center of our Helmholtz coils. As an approximation, we will take our magnetic field to be constant along the plane perpendicular to our z axis at the midpoint between our coils. While the radius and number of turns for our Helmholtz coils was not provided to us, we access the specifications provided by a retailer to obtain these values [3]. We get that the number of turns per coil is $n = 160$ and the radius/separation between the coils is $R = 14\text{cm}$.

Returning to equation 4, the last parameter we need to calculate the charge to mass ratio is the velocity of our electron beam. Calculating this velocity is relatively straightforward. Our electrons are accelerated through an electric potential V , gaining kinetic energy equal to their charge times that potential. We know the value of the supplied potential and so we can calculate the velocity (in terms of q/m).

$$qV = \frac{1}{2}mv^2 \quad (11)$$

$$\therefore v = \left(\frac{2qV}{m}\right)^{1/2} \quad (12)$$

Combining equations 4, 10, and 12 we get our final equation for e/m :

$$\frac{q}{m} = 2 \left(\frac{5}{4}\right)^3 \cdot \frac{a^2}{(N\mu_0)^2} \cdot \frac{V}{(Ir)^2} \quad (13)$$

Substituting our constants:

$$\frac{q}{m} = (1.893 \cdot 10^6 [H^{-2}]) \cdot \frac{V}{(Ir)^2} \frac{[V]}{[A^2 m^2]} \quad (14)$$

Therefore if we plot voltage versus current times radius quantity squared, the slope of our function will be proportional to q/m , shown explicitly by equation 14.

2.2 Diffraction Pattern Considerations

In analyzing the patterns produced by electrons passing through a diffraction grating we can validate the treatment of electrons as both particles and waves.

For our experiment we will use the LEAI-62 Electron Diffraction Apparatus depicted in figure 3. This device enables us to easily tune the trajectory of our electron beam via the "X-Position" and "Y-Position" knobs. These adjustments use electrostatic plates to deflect our electron beam in the horizontal and vertical directions respectively, as seen when looking at the screen. Further, we can adjust the velocity of our electron beam by adjusting the "High Voltage" knob. And lastly, we can adjust the focus and brightness of our beam using the other knobs. Our beam diffracts through a polycrystalline gold foil, resulting in a radially symmetric beam distribution incident upon the fluorescent screen.



Figure 3: LEAI-62 Electron Diffraction Apparatus.

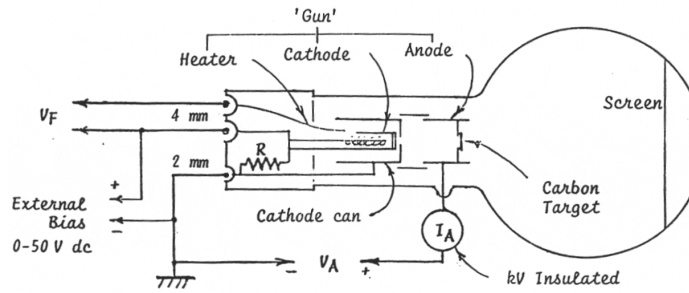


Figure 4: Schematic of typical Electron Diffraction Apparatus [2]. The key components are an electron gun, shown on the left; a target material, shown in the middle as "Carbon Target;" and a screen, shown on the right. Note that the LEIA-62 Electron Diffraction Apparatus uses a polycrystalline gold foil as a target rather than carbon.

Similar to Rutherford's initial gold foil experiment, when diffracting through the gold foil, our electron beam is probing

the geometry of the gold foil. Reversing this thought process, if we know the geometry of our gold foil, we can uncover properties of the electron.

Our polycrystalline gold foil is manufactured to be thin so that the probability of multiple scattering events is minimized. Further, the space between the gold foil and the fluorescent screen is a vacuum. Therefore, we assume our electron beam travels in a straight trajectory after its initial diffraction.

As our electrons pass through our gold foil, they diffract according the Bragg's Law. Bragg's law is the result of geometric optics and can explain the geometry of both reflections and refractions.

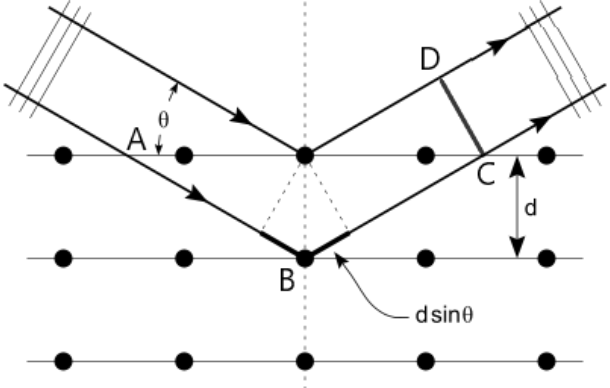


Figure 5: Geometry of diffraction through thin film with ray optics. We apply the same principles here to our electron beam, thus treating our beam as a wave. Note the angle of incidence/refraction, θ , and the spacing between adjacent planes of atoms, d .

In the case of diffraction, our electron beam is scattering off two different layers of our gold foil. The two different trajectories result in two different path lengths. If we treat our electron beam as a wave which was initially entirely in phase, it may now be shifted out of phase as a consequence of these differing path lengths. In the end, these phase shifts characterize themselves as an interference pattern which we observe on our fluorescent screen. When the path lengths of our two beams differ by half integer wavelengths they will undergo complete destructive interference. When they differ by integer wavelengths they will undergo constructive interference, resulting in high intensity beams incident upon our fluorescent screen. We can adjust the fluorescence of the screen so that only this peak intensity is visible. Following the geometry of figure 3 we can derive a relationship between our beam wavelength and the geometric pattern of its constructive peaks.

$$AB + BC - AD = n\lambda \quad (15)$$

Through simple trigonometric identities we can relate the spacing between atoms to the spacing between each layer of atoms, d , and the angle of incidence/diffraction (shown in figure 5).

$$\frac{d}{sin\theta} + \frac{d}{sin\theta} - \frac{2dcos\theta}{tan\theta} = n\lambda \quad (16)$$

A further simplification yields Bragg's Law:

$$n\lambda = 2dsin\theta \quad (17)$$

Now we must address the problem of how to relate our experimental output, a collection of rings on a screen, to our geometric results. Since we are using a polycrystalline gold foil as our target, our geometries are actually more complicated than figure 5. Yet, we can extend our simple treatment from figure 5 to the more complicated case.

The term polycrystalline indicates that there are multiple different crystal structures within our material. Each of these crystals have faces at different angles. Relative to the size of these crystal structures, the cross sectional area of our electron beam is quite large, thus it will be incident upon many faces at the same time. Further, each of these faces will result in different diffraction angles, therefore we require a systematic way of tracking these crystalline structures. Luckily, Miller indices, shown in figure 6 provide a solution for organizing these geometries. The three Miller indices (a_1, a_2, a_3) correspond to vectors in the $(a_1, 0, 0)$, $(0, a_2, 0)$, and $(0, 0, a_3)$. The face which the three Miller indices represent is the plane which these three vectors draw out.

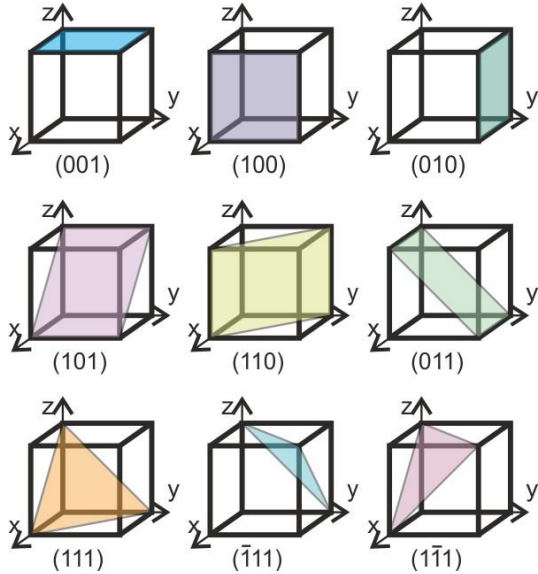


Figure 6: Visual representation of Miller indices. The labeling scheme corresponds to our Miller indices (a_1, a_2, a_3) .

With the orientation of our crystal faces properly defined, we can express the distance between two crystal planes, d , in terms of the Miller indices:

$$d = \frac{a}{\sqrt{a_1^2 + a_2^2 + a_3^2}} \quad (18)$$

where 'a' is known as the lattice constant and is known to be 0.4079 nm for gold. Combining our above equation with Bragg's Law (equation 17).

$$\lambda = \frac{2a \sin \theta}{n \sqrt{a_1^2 + a_2^2 + a_3^2}} \quad (19)$$

Finally, we can take equation 19 and apply the small angle approximation so that $2 \sin \theta = r/D$.

$$\lambda = \frac{ar}{nD \sqrt{a_1^2 + a_2^2 + a_3^2}} \quad (20)$$

$$\therefore r = \frac{\lambda n D \sqrt{a_1^2 + a_2^2 + a_3^2}}{a} \quad (21)$$

Considering the dimensions of our system ($D = 255\text{mm}$, $r_{max} = 65\text{mm}$) our approximation should be accurate to within 2%, a resolution which we would not be able to discern on our fluorescent screen.

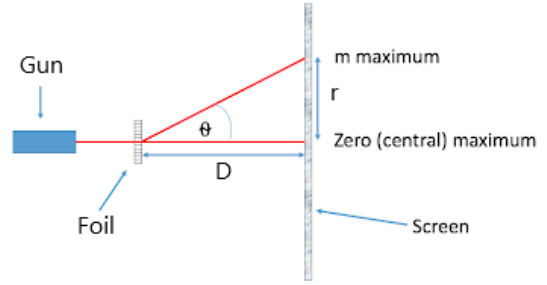


Figure 7: Representation of diffraction through medium. The distance between our foil and the screen is D , the radial distance from our on axis beam to the diffracting beams is R , and the angle of diffraction is θ

We have solved for the radii of our rings entirely using geometric optics, as such we have treated our electron beam as a wave. We now introduce the de Broglie wavelength of the electron.

$$\lambda = \frac{h}{p} \quad (22)$$

where h is Plank's constant and p is the momentum of the electrons. The electron momentum comes entirely from the acceleration of the electrons through a potential difference. This potential difference will be exactly the supplied voltage in our experiments.

$$\lambda = \frac{h}{\sqrt{2meV}} \quad (23)$$

Substituting the de Broglie wavelength into equation 21

$$r = \frac{\sqrt{2}}{2} \cdot \frac{hD}{a\sqrt{me}} \cdot n \left(\frac{a_1^2 + a_2^2 + a_3^2}{V} \right)^{1/2} \quad (24)$$

Using the following known values for constants: $h = 6.62 \cdot 10^{-34} \frac{[\text{m}^2][\text{kg}]}{[\text{s}]}$, $D = 0.255[\text{m}]$, $a = 0.4079 \cdot 10^{-9}[\text{m}]$, $m = 9.11 \cdot 10^{-31}[\text{kg}]$, and $e = 1.602 \cdot 10^{-19}$, we are now prepared to make experimental predictions for the radii of the rings produced on the fluorescent screen.

$$\frac{hD}{a\sqrt{me}} = 1.084[\text{m}][\text{V}^{1/2}] \quad (25)$$

For example, using equation 24 with Miller indices $(0,0,1)$ at 20keV we expect:

$$r = \frac{\sqrt{2}}{2} \cdot 1.084 \cdot n \left(\frac{0^2 + 0^2 + 1^2}{2 \cdot 10^4} \right)^{1/2} \quad (26)$$

$$r = n \cdot 5.42 \cdot 10^{-3}[\text{m}] \quad (27)$$

We can repeat this procedure for other Miller indices.

3 Experimental Methods

The methods used in this lab rely heavily on specialized equipment. With access to such equipment, the procedures are relatively simple.

3.1 Charge-to-mass Ratio Methods

As discussed in the theoretical considerations, in order to measure the charge-to-mass ratio we use a pair of Helmholtz coils with an electron gun positioned such that the electron beam is fired perpendicular to the magnetic field. The electron gun is inside a low-pressure helium gas chamber so that the electron path is illuminated.

We control the velocity of our electron beam by changing the input voltage to the electron gun; we control the strength of our magnetic field by changing the input current to the Helmholtz coils. By systematically altering these two parameters, and measuring the radius of the resulting electron beam, we have all the data necessary to calculate the charge-to-mass ratio.

The actual data acquisition process is completed by taking photographs of our system at each voltage-current combination. We alter the current from 0-2A in 0.25A increments and the voltage from 100V-300V in 50V increments. With these data we will be able to produce 6 linear regressions (one for each current value) corresponding to equation 14. Examples of beam behavior for various voltage-current conditions are shown in figure 10 on Page 8.

With our data captured, we go through each image and record the voltage, current, and beam radius. Note that the beam radius can not be measured for many of our images. The results of our measurements can be found in Table 1 on Page 9.

3.2 Diffraction Pattern Methods

Since we are using the LEAI-62 Electron Diffraction Apparatus, our experimental methods are greatly simplified. We turn on the device, wait some time to allow the device to warm-up, and start taking measurements. If our diffraction pattern is not centered appropriately, we use the appropriate adjustment knobs to adjust its position.

For data acquisition, we use a camera to take pictures of the diffraction pattern produced on the screen. We first start with our acceleration voltage at 8.5kV. We increment our voltage by 500V and record our data until we reach a maximum voltage of 20kV.

Throughout our measurements we must slightly adjust our focus to maintain a sharp diffraction pattern. Additionally, we must slightly adjust the screen brightness so that we can clearly see our patterns.

4 Data Analysis

4.1 Charge-to-mass Ratio Analysis

The data analysis for calculating our charge to mass ratio is also relatively straightforward. With all our data organized in an excel spreadsheet, we can directly calculate $(IR)^2$ and

then use plotting features within Excel to make 6 different plots of V vs $(IR)^2$. Each regression corresponds to a different current, yet their slopes, which are equally proportional to $\frac{e}{m}$, should be the same. The results of our data calculation can be seen in table 1 on page 9, and our regressions can be seen in figure 11 on page 10.

With each subfigure in figure 13, we can fit a linear regression to our data. From this regression we extract the slope. Due to experimental uncertainties, each figure provides us with a slightly different slope. We can take a simple average of these slopes to get a more precise result. From our data we get the average slope to be $2.8 \cdot 10^4 [V]/[A^2 m^2]$.

Finally, using equation 14 we can input our slope value to obtain our charge to mass ratio, which we will know rename $\frac{e}{m}$, since we have calculated the charge to mass ratio specifically for an electron. Additionally, although we have not proved it in this experiment, we know the charge of an electron is negative and so we will negate our result.

$$\frac{e}{m} = -(1.893 \cdot 10^6 [H^{-2}]) \cdot 2.8 \cdot 10^4 \frac{V}{A^2 m^2} \frac{[Am]}{[V^2]} \quad (28)$$

$$\frac{e}{m} = -5.3 \cdot 10^{10} \frac{[C]}{[kg]} \quad (29)$$

The known value of the electron charge to mass ratio is $\frac{e}{m} = -1.76 \cdot 10^{11} [C]/[kg]$. As such our calculated value is approximately 3.3 times, or 70%, smaller than the actual value.

While there are undoubtedly many sources of error, we suspect our largest error comes from our calculations of the magnetic field produced by our Helmholtz coils. We follow the ideal approximation for the magnetic field produced by Helmholtz coils. However, looking at the product description from the distributor of our Helmholtz coils [3], it is stated that with our apparatus the charge to mass ratio of an electron is

$$\frac{e}{m} = 8 \cdot \frac{V}{B^2 r^2} \frac{[C]}{[kg]} \quad (30)$$

This is in direct contradiction with our results depicted in equation 13.

$$\frac{q}{m} = 2 \left(\frac{5}{4} \right)^3 \cdot \frac{a^2}{(N\mu_0)^2} \cdot \frac{V}{(Ir)^2} = 2 \cdot \frac{V}{B^2 r^2} \frac{[C]}{[kg]} \quad (31)$$

We can multiply our result by a factor of 4 to account for this discrepancy. Therefore we get:

$$\frac{e}{m} = 4 \cdot -5.3 \cdot 10^{11} = -2.12 \cdot 10^{11} \frac{[C]}{[kg]} \quad (32)$$

With this new result our error is reduced to 20%, which is undoubtedly much better. But, we must now ask where this additional factor of 4 (in equation 32) comes from. Equation 32 suggests that either the Voltage is 4 times larger than expected, or the magnetic field is 2 times weaker than expected. Perhaps, the problem is some weird combination of the two. Without a better understanding of the details of the Helmholtz coil and electron gun we may not be able to answer this question. Perhaps, the measured voltage is actually twice the supplied voltage, which would lead to the magnetic field being halved. Perhaps it is something else. All potential problems culminate in our calculation of the magnetic field, since we have proven it is inaccurate.

4.2 Diffraction Pattern Analysis

While our data collection was straightforward, our analysis is quite tedious. We must go through each frame and record the radii of our different diffraction pattern. An example of several images collected for different acceleration voltages can be seen in figure 12 on 11. We will first use our 20kV image to map the rings labeled in figure 9. Using the fact that the diameter of our screen is 130mm, we can digitally include a ruler into our image. We can then measure the radii of our rings. We get the following measurements:

$$r_a \approx 16.5\text{mm}, r_b \approx 25.5\text{mm}, r_c \approx 32\text{mm} \quad (33)$$

Using equation 24, and assuming we are measuring the first order diffractive beam ($n = 1$), we can create a table for all our different possible ring radii using the different combinations of Miller indices. We can then divide our measured radii by these values to determine which Miller indices our ring corresponds too. This procedure is captured in the table below.

Unique Roots	Radius	r_A/radius	r_B/radius	r_C/radius
1	0.00542	3.044280443	4.70479705	5.90405904
1.414213562	0.007665	2.152631345	3.3267939	4.17480018
1.732050808	0.009388	1.757616133	2.71631584	3.40871008
2	0.01084	1.522140221	2.35239852	2.95202952
2.236067977	0.012119	1.361443603	2.1040492	2.64037547
2.449489743	0.013276	1.242822286	1.92072535	2.41032201
2.828427125	0.01533	1.076315672	1.66339695	2.08740009
3	0.01626	1.014760148	1.56826568	1.96801968
3.16227766	0.01714	0.962686004	1.48778746	1.8670274
3.31662479	0.017976	0.91788509	1.41854968	1.78014078
3.464101615	0.018775	0.878808067	1.35815792	1.70435504
3.605551275	0.019542	0.844331479	1.30487592	1.63749135
3.741657387	0.02028	0.813618172	1.2574099	1.57792615
4	0.02168	0.761070111	1.17619926	1.47601476
4.123105626	0.022347	0.73834646	1.14108089	1.43194465
4.242640687	0.022995	0.717543782	1.1089313	1.39160006
4.358898944	0.023625	0.698405832	1.07935447	1.35448404
4.472135955	0.024239	0.680721801	1.0520246	1.32018774
4.69041576	0.025422	0.649042771	1.0030661	1.25874962
4.898979486	0.026552	0.621411143	0.96036268	1.20516101
5.196152423	0.028163	0.585872044	0.90543861	1.13623669
5.196152423	0.014082	1.171744089	1.81087723	2.27247338

Figure 8: Above table for fitting rings to various Miller indices. The column "Unique Roots" corresponds to unique combinations of $\sqrt{a_1^2 + a_2^2 + a_3^2}$. We then use equation 24 to calculate our expected radii. Finally we divide our measured ring radii by our expected radius for each unique root. We match our ring to the unique root which corresponds with a final ratio of approximately 1. Examples of Miller indices corresponding to the unique root 3 are (2,2,1), (2,1,2), (1,2,2), (3,0,0), etc.

Having done this calculation, we can only determine potential Miller indices for our three rings. It would be more accurate to say that we know the square root of the sum of the squares of our Miller indices. Let $A = \sqrt{a_1^2 + a_2^2 + a_3^2}$

A_A : 2.821, 3, or 3.162

A_B : 4.472, 4.690, or 4.899

A_C : 5.196

Regardless of the specific Miller indices, we should now be able to predict the radii of our rings as functions of the applied voltage following equation 24 with $n=1$.

$$V = \frac{1}{2} \cdot \frac{h^2 D^2 A^2}{a^2 me} \cdot \left(\frac{1}{r}\right)^2 \quad (34)$$

Plotting voltage vs $(1/r)^2$ for our three rings we get figure 13. From calculating the constants in 34 we get the expected slopes 4.7, 11.8, and 15.9 for rings A, B, and C respectively. With our data we measure slopes of 5.6, 5.8, and 35.1; these slopes correspond respectively to errors of 19%, 50%, and 120%.

With such large errors our experiment does not confirm our theoretical calculations. This will be discussed in our conclusion.

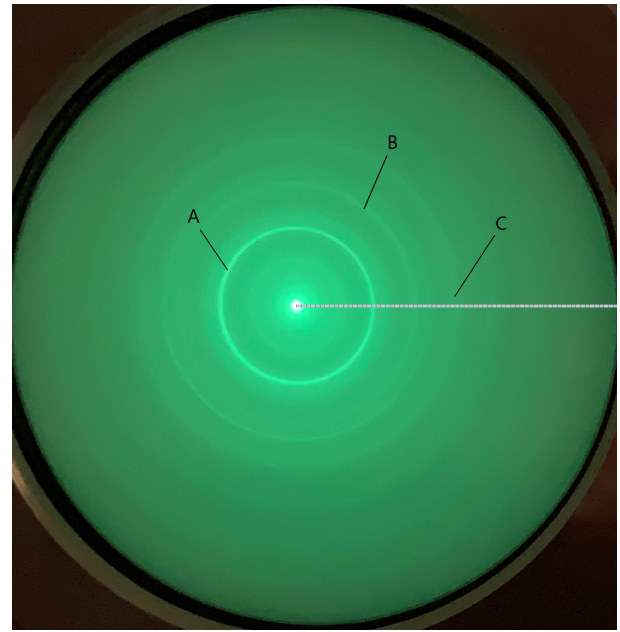


Figure 9: Diffraction pattern with a 20kV electron acceleration voltage. Three distinct diffraction rings are labeled: A, B, and C. The radii of these rings can be measured digitally since we know the total diameter of the screen is 130mm.

5 Conclusion

Throughout this lab we have conducted various measurements highlighting the properties of the electron. Namely we calculated the charge to mass ratio of the electron and also related diffraction rings to the properties of the electron.

Our final result for the charge to mass ratio is $\frac{e}{m} = -2.12 \cdot 10^{11} \frac{[C]}{[kg]}$. As stated in our analysis, this is 20% greater than the actual value of $\frac{e}{m} = -1.6 \cdot 10^{11} \frac{[C]}{[kg]}$. Further, we were not able to achieve this value from our theory alone. We rely on external documentation that the charge to mass ratio calculated with our Helmholtz coils is 4x larger than expected. It is not clear where this discrepancy comes from, a few potential causes are stated in our analysis. With that aside, our 20% error is still reasonably large and most likely due to experimental error. Our method for measurement is not the

most precise, considering many times our ruler does not pass through the center of the circular arcs. Further, for many voltage/current configurations, the electron beam would not stay within our glass bulb - as such we could not collect data for those points. Lastly, the electron beam diverges considerably fast. As such, we can not be precise in our measurements when the beam itself is approximately 1cm wide.

We could improve this experiment by having a more precise measure of our magnetic field. While we have access to a magnetic probe, we cannot measure the magnetic field along the path of our electron beams. It would be helpful to first map out the magnetic field between the two coils, and then conduct our experiment as previously done. Additionally, having a larger glass bulb would allow us to record more data points to hopefully reduce our error. Additionally, however, since the magnetic field is only approximately uniform near the central axis connecting our two coils, this would require a larger pair of Helmholtz coils.

Despite our error, our final result is of the correct order of magnitude, which is quite impressive for simple measurements with a ruler. Through this experiment we demonstrate that we can accurately treat the electron as a charged particle which deflects through a magnetic field.

For our diffraction experiment, we have less quantitative success than our Helmholtz coil experiment. We are able to deduce potential Miller indices for three of the diffraction rings produced, but fail to confirm these results.

With our calculations we attempt to predict the radii of the diffraction rings as functions of acceleration voltage. We reduce this relation to a linear dependence and calculate our expected slopes using known physical constants. Then, we fit a linear regression to our data and calculate our slopes with experimental data. For the three diffraction rings tested, we calculated errors of 19%, 50%, and 120%. Therefore, our experiment fails to confirm our theoretical calculations.

The largest known source of error in this experiment is when reading our data. It is very difficult to discern what is a diffraction ring and what is not. Further, our diffraction rings become increasingly faint with increased radius, even when the brightness/focus is adjusted. Improvements to this experiment could be to use more sophisticated software to track the diffraction rings. Additionally, while, the fluorescent screen is great for visualizing our results, in general it is not the best for measurements. In place of our screen, we could construct a device which behaves like a photodiode (but for electrons) and scans across our diffraction rings. This would immediately produce data from which various peaks in intensity would correspond to our diffraction rings.

Despite the quantitative failure of this experiment, it is very successful qualitatively. We were able to describe an electron behavior using only geometric optics. As the voltage of our electron beam increases, the radii of our diffraction rings increase, as they do in our calculations. We must not get too disheartened by our large errors, for this experiment demonstrates that an electron can behave as a wave.

Combining the two experiments detailed in this report, we see the wave-particle duality of the electron. Our overall understanding of the electron has come a long way since it was first discovered in the 19th century. Its properties are truly remarkable.

References

- [1] Measuring e/m (vertical scale method). https://www.austincc.edu/mmcgraw/Labs_2426/6A-E-over-M%2006-11-13.pdf, 2006.
- [2] Ucsc physics demonstration room: Electron diffraction apparatus. `howpublished="\url{https://history.aip.org/exhibits/electron/jjinfo.htm}"`, , 2021.
- [3] SES Instruments. E/m experiment, emx-01 "retailer website". <https://www.sesinstruments.in/e-m-experiment-emx-01-5137512.html>, 2021.
- [4] James Trefil Sharon Bertsch McGrayne, George F. Bertsch. Atom - discovery of electrons, 2021.
- [5] Kent W. Staley. The discovery of the electron. <https://history.aip.org/exhibits/electron/jjinfo.htm>, 1997.
- [6] G. P. Thomson. Diffraction of cathode rays by a thin film, 1927.

Appendix

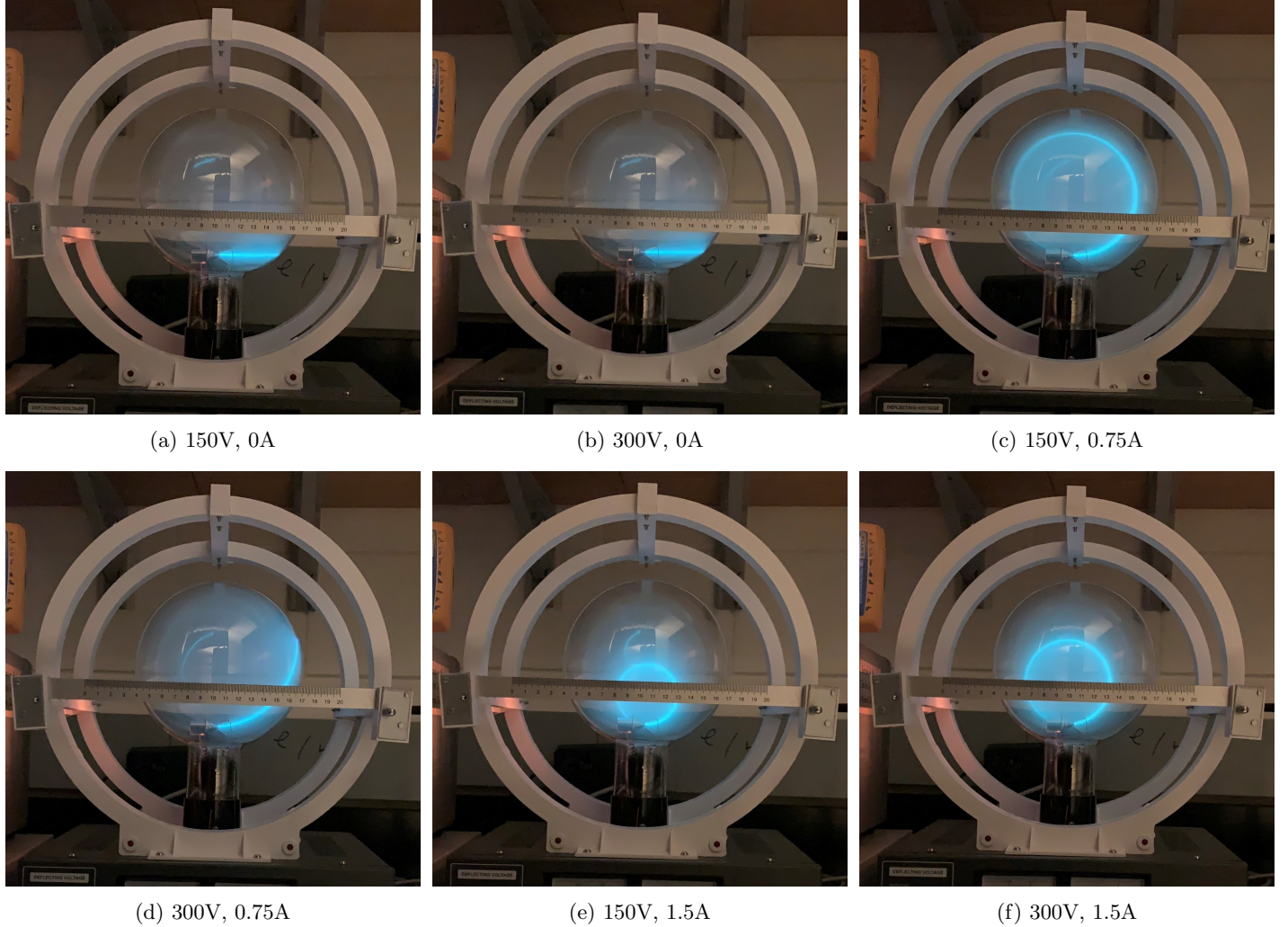


Figure 10: Example images of the data captured for measuring the charge to mass ratio of the electron. As seen in (a), for many trajectories it is impossible to measure the radius of our beam. However, for others such as (f) the beam diameter is very clear.

Voltage (V)	Current (A)	Radius (cm)
100	0.75	7.8
100	1.0	5.7
100	1.25	4.7
100	1.5	3.9
100	1.75	3.3
100	2.0	2.9
150	0.75	9.7
150	1.0	7.2
150	1.25	6.1
150	1.5	4.8
150	1.75	4.1
150	2.0	3.7
200	0.75	11.1
200	1.0	8.3
200	1.25	6.6
200	1.5	6.1
200	1.75	4.8
200	2.0	4.2
250	1.0	9.5
250	1.25	8
250	1.5	6.2
250	1.75	5.3
250	2.0	4.1
300	1.0	10.6
300	1.25	8.2
300	1.5	6.8
300	1.75	5.8
300	2.0	5

Table 1: Results of our Helmholtz coils experiment. Used in plotting figure 13.

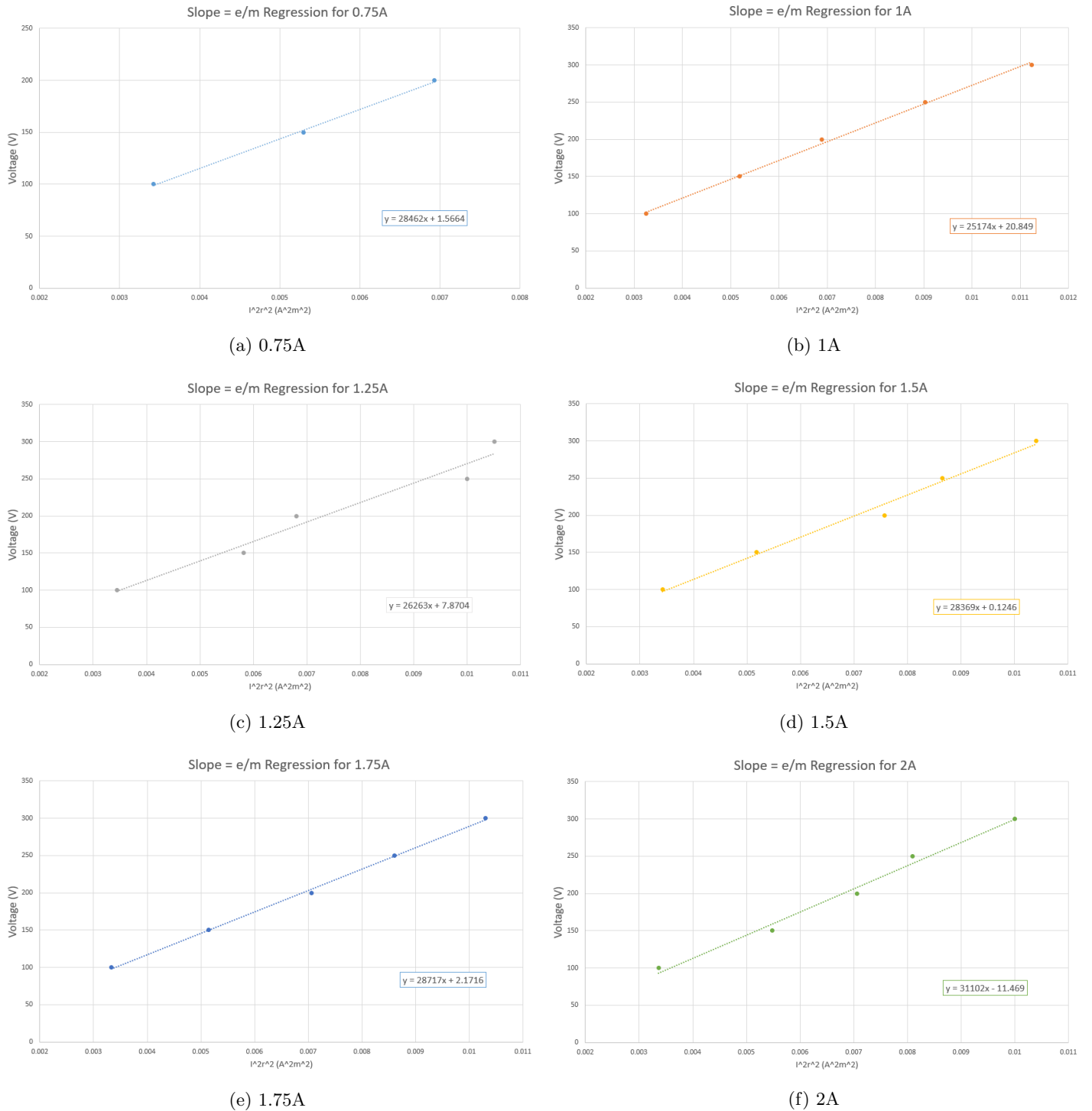


Figure 11: Various regressions plotting the Voltage supplied to our Helmholtz coils vs the combined parameters I^2r^2 . The slopes of these regressions are directly proportional to $\frac{e}{m}$, note that they are all consistent with each other. The data for these graphs comes from table 1.

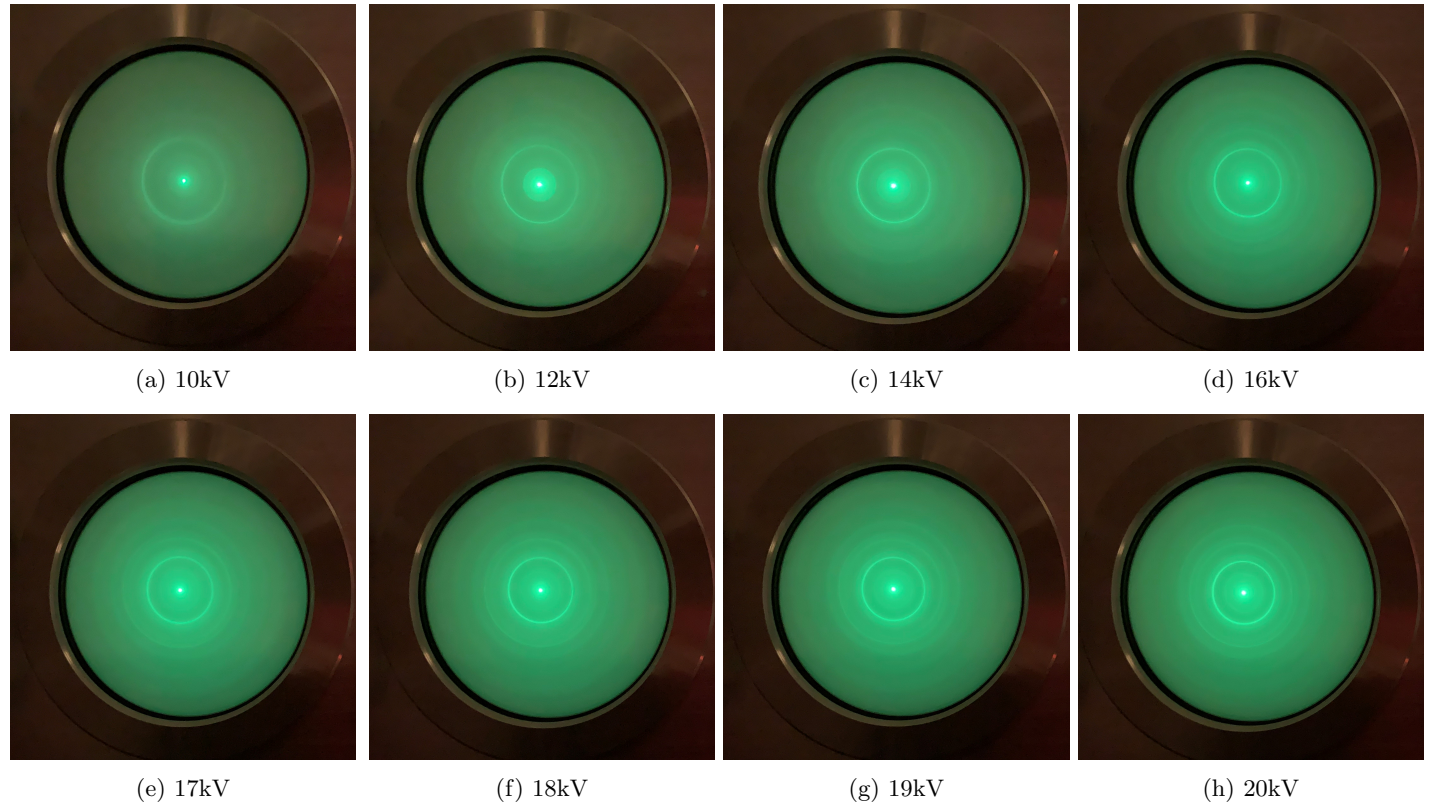


Figure 12: Diffraction rings produced by the LEAI-62 Electron Diffraction Apparatus for various electron beam acceleration voltages. Note that many rings are unable to be seen at lower voltages.

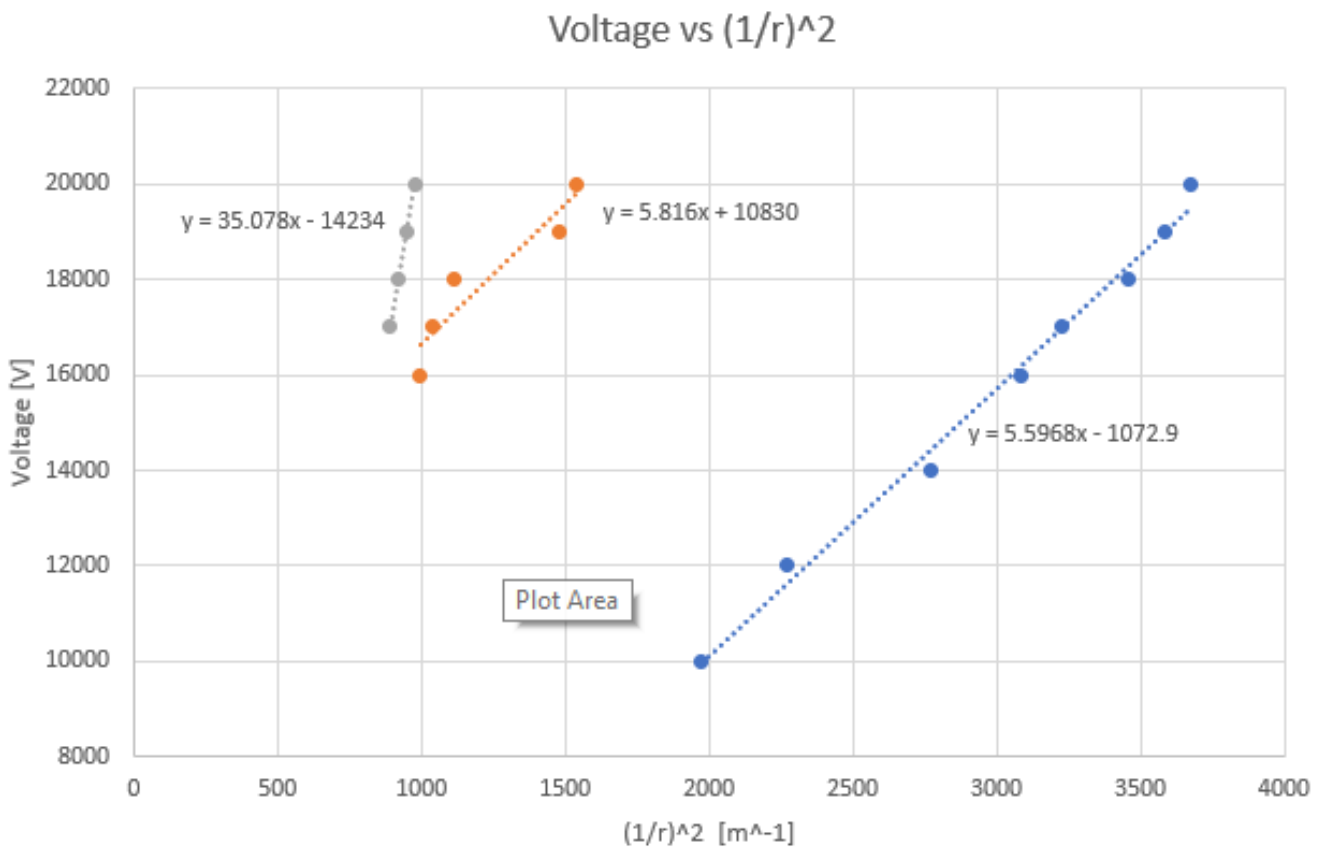


Figure 13: A plot relating our ring diameter to our applied electron acceleration voltage for rings A, B, and C, defined in our analysis. There are fewer data points for rings B and C because the further away from the center of the display a ring is, the more blurred it is, until it is no longer possible to discern a ring anymore. The data points shown correspond to the 8 images in figure 12.